51st IEEE Conference on Decision and Control
December 10-13, 2012. Maui, Hawaii, USA

Fast scanning in AFM using non-raster sampling and time-optimal trajectories

Peng Huang[1] and Sean B. Andersson[2]
[1,2]Department of Mechanical Engineering and [2]Division of Systems Engineering
Boston University, MA 02215

***Abstract*— Standard approaches to high-speed AFM rely on moving the tip faster along the raster-scan pattern. Recent work has developed a non-raster scheme for string-like samples such as biopolymers that reduces imaging time by reducing the total number of measurements. This *local raster-scan* algorithm steers the tip in a sinusoidal path along the sample, acquiring only data near the sample of interest. It has been shown that for a particular class of samples, an order-of-magnitude reduction in imaging time is possible. In this paper we build upon that approach but consider time-lapse imaging. In this scenario, the prior knowledge from previous images can be used to setup a time-optimal control problem between successive crossing points along the string-like sample. Using recent results in time-optimal control, we solve this problem and illustrate that it can, in principle at least, yield at least an additional order of magnitude improvement in the imaging rate.**

I. INTRODUCTION

Studying the dynamics of single macromolecules continues to further our understanding of biomolecular systems and to elucidate a wide variety of genetic diseases [1], [2]. There are many techniques available, including fluorescence microscopy [3], [4], optical techniques [5], optical traps [6], electron microscopy [7] and atomic force microscopy (AFM). Among these tools, AFM provides a unique set of capabilities, including the ability to observe systems in their physiological environment, a resolution on the order of nanometers or better, and the ability to measure mechanical properties directly. As a result, it has been playing an essential role in the study of a wide variety of macromolecular systems. Examples include direct observation of directional transport by protein motors [8], interactions between proteins [9], [10] and other cellular behaviors [11].

One of the primary drawbacks of AFM when applying it to the study of dynamic processes is its slow imaging rate, with commercial instruments typically taking seconds to minutes to acquire a single frame. Because of the impact improved imaging rates can have in the study of biomolecular systems and in other areas such as metrology and materials science, a great deal of effort has been made on addressing this problem and near video-rate speed has been achieved [12]. Approaches to high-speed AFM that have been pursued include improvements of the mechanical components [13], advanced controller designs for the piezo actuators [14] [15] and other approaches such as using tuning forks for fast scanning [16] and novel detection-based approaches for imaging based on the transient response [17]. Despite these achievements, there is a need for even faster imaging over larger scan areas. For example, the dynein motor has been reported to move at speeds of up to 1.7 μm per second. Even at 30 frames per second, the motor would take more than six steps between the start and end of imaging a single frame. To study such high speed systems, an alternative approach is needed.

This work was supported in part by NSF through grant CMMI-0845742 and by grants from the Natiional Center for Research Resources (5R21RR025362-03) and the National Institute of General Medical Sciences (8 R21 GM103530-03) from the National Institutes of Health.

II. OVERVIEW OF OUR APPROACH

In prior work the authors (with others) have introduced a *local raster-scan* technique that reduces imaging time for string-like samples such as biopolymers [18]. The algorithm, described in Sec. II-A below, uses the measurements in real time to steer the tip of the AFM along the sample, focusing the measurements in the region of interest. Here we build upon that algorithm and consider high speed time-lapse imaging of such samples. Prior knowledge in terms of non-raster data taken from previous scans can be utilized to produce the time optimal path to maximize the imaging rate. In this section, we begin with a brief description of the local raster scan algorithm. From there we formulate our problem into time optimal control with fixed initial and end conditions.

A. Local raster scan algorithm

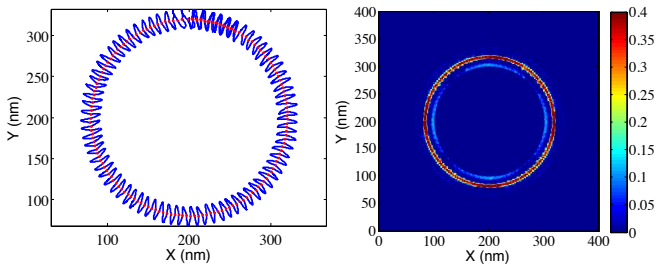

(a) Tip trajectory (b) Imaging result

Fig. 1. Illustration of the local raster algorithm. (a) The string-like sample (red line) curves in a "circle" pattern; the local raster algorithm dithers the tip in a sinusoidal pattern, using the measurements to track the sample (blue line). (b) Interpolation is used to generate images from the non-raster data.

The primary motivation for the local raster-scan algorithm is high-speed imaging of dynamics along biopolymers. In this method, illustrated in Fig. 1(a), the tip is steered along a sinusoidal path transversely to the string. Each time the tip moves from substrate to sample or sample to substrate, the algorithm updates its prediction of the path of the sample, modifying the sinusoidal pattern to stay along the sample. An example of a simulation run is shown in Fig. 1(a). The simulation includes the dynamics of the scanning stage, the tip and cantilever, the nonlinear tip-sample interaction, and noise typical in measurements. (Details on the simulation setup can be found in [18].). We have also developed a scheme for producing images from the local raster scan data in [19]; the result from the simulated run is shown in Fig. 1(b). Depending on the details of the sample, the imaging rate can be improved by an order of magnitude or more.

B. Problem description

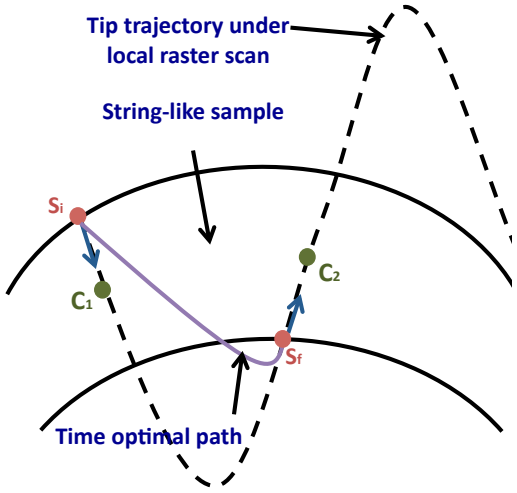

Fig. 2. Illustration of the tip trajectory under the local raster scan and the time optimal trajectory. The local raster-scan algorithm drives the tip in a sinusoidal pattern (dashed black) transversely to the sample (solid black). S_i and S_f (red) are the initial and final states with full knowledge including the position and the velocity. C_1 and C_2 (green) are the measurements on the centerline of the sample which are used here to determine the velocity of S_i and S_f. Given a pair of initial and final states, the time optimal path can be derived illustrated in purple.

In this paper we assume that we have an initial scan along a biopolymer; this scan establishes a sequence of crossing points. Our goal is to move transversely across the sample from crossing point to crossing point as quickly as possible. A single crossing sequence is illustrated in Fig. 2. In this figure, C_1 and C_2 denote points on the centerline of the string-like sample while S_i and S_f represent points of transition on the different sides of the sample. Given our assumptions, these points are known exactly from the previous local raster-scan (shown in dashed-black on the figure). There are clearly many other paths between the points S_i and S_f that would be suitable for a local-raster scan; all that is needed is that from an initial point at S_i with a velocity vector pointing toward C_1, the system end at S_f with a velocity vector pointing toward C_2. Our basic problem, then, is to find the time-optimal trajectory that satisfies the given boundary conditions. A full scan of the sample can then be accomplished by driving the tip to follow the time optimal paths connecting the sequence of crossings along the string-like sample. Note that the resulting entire trajectory is a combination of each local optimal trajectory and is not necessarily a globally optimal solution.

Scanning in AFM is typically done with piezo actuators using either a piezo tube or a frame-in-frame style scanner [20]. In modeling the positioning mechanism, both dynamics [21] and nonlinearities including hysteresis [22] and creep [23] should be taken into account. While such effects are important, we will assume a linear model for this paper. In practice, one could have a (even lower level) controller to handle nonlinearities, though more practically our approach will need to be modified to directly account for them.

It has been shown that a single mass-spring-damper is a reasonable model for the dynamics of a piezo [22] and we take such a model here. For the sake of simplicity, we utilize the same linear dynamics model for the actuators in both the $X-$ and $Y-$ directions and ignore the cross coupling between axes. Such an assumption is reasonable for a frame-in-frame style scanner.

With these assumptions in place, our problem then becomes one of finding the time-optimal controller to transition a second-order linear time-invariant system between two points in its state space. This is a well-known problem that can be solved using the Pontryagin Maximum Principle (PMP) [24]. In the next section we briefly describe recent results in the time optimal control of such systems and then use those results in our application.

III. Time-optimal control of second-order systems

The time optimal control of linear time-invariant systems was considered at least as far back as Pontryagin's seminal work on his maximum principle [24]. As described below, that approach yields a bang-bang control law based on a switching curve in the state space. Finding that switching curve, and thus the switching time, is in general computationally challenging. Recent results for second order systems have yielded a more efficient approach based on mapping the problem to a coordinate system in which the switching curve is made up of segments of standard spirals. Below we outline the scheme; details can be found in [25].

A. Problem formulation and the bang-bang solution

Consider a second-order system of the form

$$G(s) = \frac{\omega_n^2}{s^2 + 2\zeta\omega_n s + \omega_n^2}.$$

The time-optimal control problem can be formulated as follows:

$$\min J = \int_0^{t_f} dt. \qquad (1)$$

subject to

$$\dot{x} = \begin{pmatrix} 0 & 1 \\ -\omega_n^2 & -2\zeta\omega_n \end{pmatrix} x + \begin{pmatrix} 0 \\ \omega_n^2 \end{pmatrix} u, \tag{2}$$

$$x(t_0) = x_0, \qquad x(t_f) = x_f, \tag{3}$$

where we have expressed the system in state space form. We assume that the system has a pair of stable complex conjugate poles and that the admissible control is in the range of $u \in [u_{\min}, u_{\max}]$.

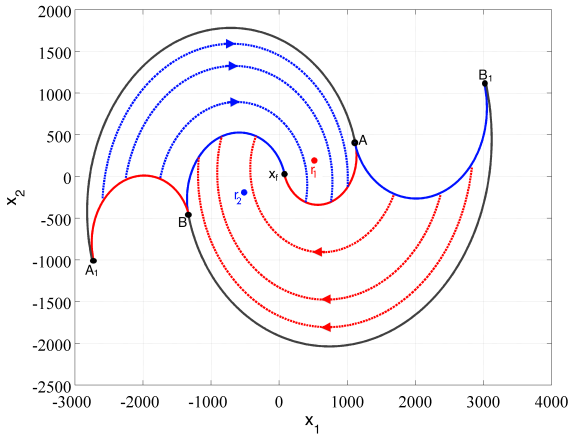

Fig. 3. Illustration of the construction of the switching curve in state space. x_f is the final state. x_fA and x_fB are the final switching curves derived by evolving the system backwards in time under the control $u_{\max}$ and $u_{\min}$ respectively; Other components of the switching curve such as BA_1 and A_1B are produced by rotation and scaling of x_fA and x_fB.

Appealing to the PMP, the optimal solution can be shown to be bang-bang. That is, the system should first apply one extreme of the control for a given amount of time, then switch to the other extreme for another period of time, and so on until the target is reached. The point at which switches occur is defined by the *switching curve*. This curve divides the state space into two distinct regions; the positive control extreme is applied on one side of the curve and the negative control extreme on the other. Constructing this switching curve, however, is non-trivial. As shown in Fig. 3, for example, the final switching curves (x_fA and x_fB) are derived by evolving the system backwards in time from the target (x_f) under the control $u_{\max}$ and $u_{\min}$ respectively. Other components of the switching curves can be then produced by rotating and scaling the final switching curve. Construction of the curve is in general a non-trivial computation step. Similarly, determining the switching time (or times) is computationally challenging since it involves knowing when a trajectory has crossed the (numerically computed) switching curve.

In the following section, we describe recent work from [25] in which a convenient mapping is derived that simplifies the process of constructing the switching curve as well as computing the switching time.

B. A useful coordinate transformation

Consider a second order system of the form (2) but expressed in a different coordinate system. This new coordinate system is built from the following mapping. We define

$$a_1 = 2\zeta\omega_n,$$
$$a_2 = \omega_n^2,$$

and let

$$Ax_r + Bu_{\max} = [v, \quad z]^T, \tag{4a}$$

$$Ax_r + Bu_{\min} = [m, \quad n]^T. \tag{4b}$$

Then we define a mapping $M_{min} : \mathbb{R}^2 \to \mathbb{R}^2$,

$$x \mapsto X = A_{\min}^{-1}(x - B_{\min}), \tag{5}$$

in which

$$R(t) = e^{\frac{a_1}{2}t}, \tag{6a}$$

$$X(t) = (R(t)\cos(\omega t), R(t)\sin(\omega t))^T, \tag{6b}$$

$$A_{\min} = \begin{pmatrix} -\frac{a_1 m + n}{a_2} & -\frac{m(4a_2 - a_1) - 2a_1 n}{4a_2\omega} \\ m & -\frac{a_1 m + 2n}{2\omega} \end{pmatrix}, \tag{6c}$$

$$B_{\min} = x_f + \left(\frac{a_1 m + n}{a_2}, \quad -m\right)^T. \tag{6d}$$

Under this mapping the switching curve becomes a collection of similar spirals. The detailed structure of that curve depends on the type of target point. Here we consider *holdable equilibrium points* defined as follows.

Definition 1: A target state x_r is called a holdable equilibrium target state if $\exists\ u_o \in [u_{\min}, u_{\max}]$ such that $Ax_r + Bu_o = 0$. ∎

The condition $Ax_f + Bu_{\max} \neq 0$ and $Ax_f + Bu_{\min} \neq 0$ should be satisfied to guarantee the existence and effectiveness of the mapping, meaning that x_f should be reachable under the control $u_{\max}$ and $u_{\min}$.

The benefit of introducing this mapping is that the switching curves become regular spirals. This structure facilitates the computation of the switching time. An example is shown in Fig. 4. The figure illustrates an initial condition (x_i) from which only a single switch (at S) is needed. The switching time is then defined by two angles, α and β. The acceleration and deceleration time is then given by these two angles. These angles can be found using a simple numerical scheme.

C. Application to non-raster scanning in AFM

The approach to solve for our time-optimal trajectory is now clear. Given a initial state x_i and final state x_f on opposite sides of the strand being imaged (as illustrated in Fig. 2), let the corresponding coordinates in the new system by denoted (X_o, Y_o) and (X_f, Y_f) respectively. As illustrated in Fig. 6, the two points are "close" in the state space and thus a single switch is expected (although the technique can handle an arbitrary number of switches). The switching time is then found using the method outlined above. After the transition, the end point becomes the new initial condition, the next

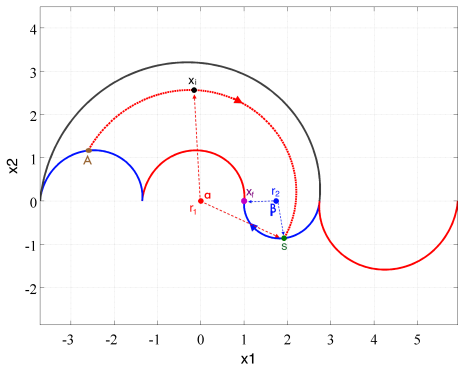

Fig. 4. Illustration of constructing the switching curve in the new coordinates. x_f is the final state. AS is a system trajectory under control $u_{\min}$ passing through the initial state x_i. $\alpha = \angle x_i r_1 S$ and $\beta = \angle x_f r_2 S$.

(desired) crossing point becomes the new target point, and the process repeats.

In principle, the entire path, including all the switching times can be calculated in advance. In practice, however, each switch should be calculated after the previous motion has been completed to prevent errors from growing throughout the scan. These errors arise from model mismatch, noise and the chattering of bang-bang control.

IV. Simulation Result

To illustrate our approach, we performed a simulation to generate the time optimal path for a second order system given the boundary conditions corresponding to adjacent crossing positions from a local raster scan of a biopolymer. We choose a model which (loosely but reasonably) approximates a piezo tube (see, e.g. [12]). In particular, for each axis, we choose a resonant frequency of $f = 871$ Hz ($\omega_n = 5.47 \times 10^3$ rad/sec) and a damping of $\zeta = 0.1282$. In addition, the accessible range of the scanner is set to be from -10μm to 10μm with the drive voltage in the range of -10 V to 10 V. As discussed in the last section, for simplicity we ignore the cross-coupling between the two axes and use the same model for both $X-$ and $Y-$axes. The Bode plot is shown in Fig. 5.

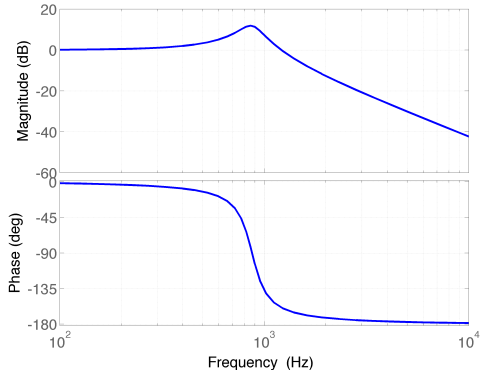

Fig. 5. The Bode plot for the model of each axis of the piezo actuator.

In [18], this model was used to simulate the local raster scan of a sample with a tip speed of 20 μm/sec. In order to compare to that result, we set the tip speed at the beginning and end points of our time-optimal problem to also be 20 μm/sec. A pair of successive crossings produced from a run of local raster scan were selected arbitrarily. These points were $x_{o_x} = [201.7, 5747]^T$, $x_{o_y} = [202, -1915.7]^T$ and $x_{r_x} = [205.85, 1831.4]^T$, $x_{r_x} = [197.95, 1991.6]^T$. The units in the state variables are nanometers and nanometers/second respectively.

In order to apply the results described in Sec. III-B, we must ensure the target point (X_f, Y_f) is a holdable equilibrium point. Consider just the motion in the x–direction. The state space model of the piezo actuator is

$$\dot{x} = \begin{pmatrix} 0 & 1 \\ -2.9 \times 10^7 & -1.4 \times 10^3 \end{pmatrix} x + \begin{pmatrix} 0 \\ 2.9 \times 10^7 \end{pmatrix} u. \tag{7}$$

With this model it is easy to show that in fact there does not exist a $u_o \in (u_{\min}, u_{\max})$ such that $Ax_{r_x} + Bu_o = 0$. Thus the target point is *not* a holdable equilibrium point. The target speed of 20 μm/sec, however, is quite slow relative to the maximum speed achievable by the system. As a result, we can approximate it by zero. Under such an approximation, the target is a holdable equilibrium point. A similar argument holds for the y–axis actuator.

Applying the mapping established in Sec. III-B, initial and target points become $X_0 = [0.9996, 0.0001]^T$, $X_f = [1, 0]^T$ and $Y_0 = [1.0003, -0.0007]^T$, $Y_f = [1, 0]^T$. These points and the switching curve (in terms of regular spirals) are shown in the new coordinate system in Fig. 6. The initial positions (black dots) seen in the zoom in plot fall in the domain of only one switch for both of the stages. For the X–stage, the system experiences acceleration ($u_{\max}$, blue) first then decelerates ($u_{\min}$, red) to its final state; for the Y–stage it decelerates ($u_{\min}$, red) from the starting point to achieve the opposite direction of the velocity and switches to the accelerating process ($u_{\max}$, blue) until arriving the target. This entire process for both of the two stages can be shown in Fig. 7. Computing α and β numerically yields a switching time of 3.792 μs, and a total travel time of 7.227 μs for the X–stage; a switching time of 3.584 μs and a total travel time of 7.427 μs for the Y–stage. Note that X–stage accomplishes its transition faster than the Y–stage in theory. In the simulation, we artificially limit the maximum command to the faster direction (or, equivalently, scale time) to ensure that they finish at the same time. The transition time is then 7.427 μs time. The time optimal tip trajectory is generated as shown in Fig. 8.

The two crossing points x_i and x_f are approximately 4 nm apart. Since most biopolymers have the same width along their entire length, one can assume that the time between any successive crossings spaced 4 nm apart will be essentially the same. Thus, using this approach, a 1 μm-long string can be scanned in approximately 2 ms for a corresponding frame rate of 500 Hz. This should be compared to the local raster-scan which can achieve approximately a 10 Hz

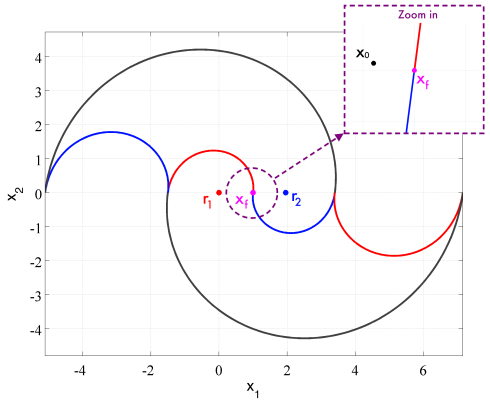

(a) Switching curves in the normal space for X–stage

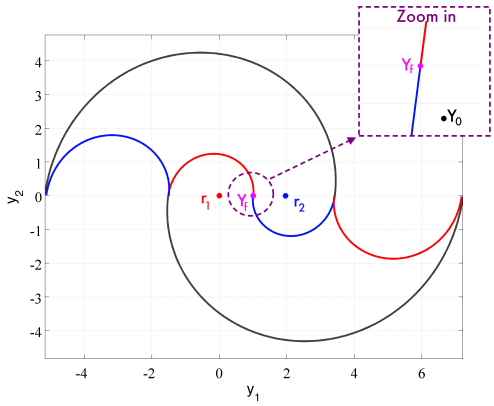

(b) Switching curves in the normal space for Y–stage

Fig. 6. Simulation result of the switching curve in the normal space for X– and Y–stage. The initial position are the black dots (shown in the zoomed image).

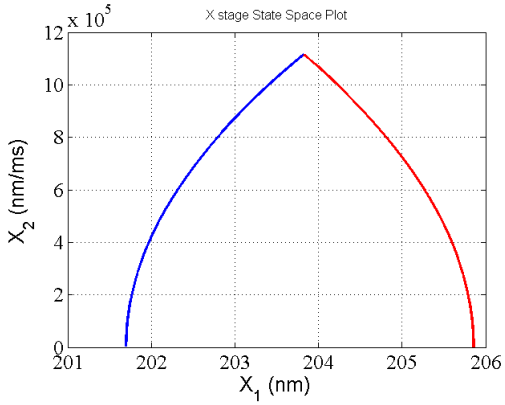

(a) State Space plot for X–stage

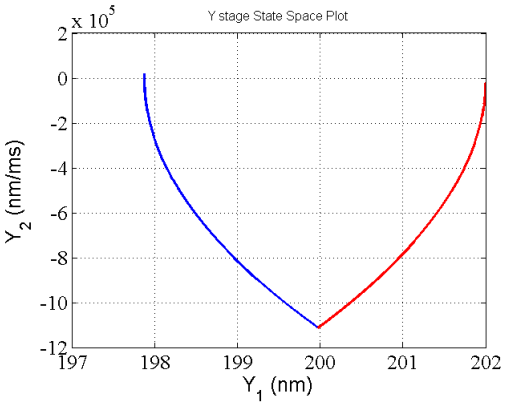

(b) State Space plot for Y–stage

Fig. 7. Simulation result of the switching policy for both X– and Y stages.

frame rate under the same conditions on the actuator, image resolution, and scan length, and to a standard raster scan which can achieve approximately a 1 Hz frame rate for the same conditions.

A. Discussion

The possible increase in frame rate to 500 Hz is quite enticing but should also be viewed as an upper limit (under the conditions stated). A comprehensive evaluation of the performance of this time optimal scanning is needed after being implemented and one should keep in mind that our approach makes several simplying assumptions. In addition, due to the nature of bang-bang control, chattering would be caused by any external disturbances or unmodeled dynamics of the system. Therefore, at the very least a robust time-optimal control scheme such as proximate time-optimal systems (PTOS) [26] must be used. These schemes trade off optimality for robustness, reducing the achievable frame rate. Another consideration is the response speed of the scanner in the z–direction. For imaging, and to avoid damage to the sample, the z-system must respond significantly faster than the rate at which features are being encountered by the tip. Since the scheme we discussed in this paper drives the tip onto and then off a sample approximately every 8 μs, features are coming at a rate of 2/(8 μs) or 250 kHz. The typical bandwidth of a z-controller is on the order of a single kHz [20]. However, recent results in this area have yielded a dual-stage z-system with a bandwidth in excess of 150 kHz [27]. That rate is fast enough to bring the time-optimal approach into the realm of feasibility. The

V. CONCLUSIONS

In this paper we have considered the problem of time-optimal transfer between two points on either side of a biopolymer or other string like sample. This problem forms the foundation for the fastest possible scan along such a sample, thus maximizing the frame rate. Simulation results indicate an improvement of nearly two orders of magnitude over a standard raster-scan scheme.

The results, however, should be viewed as a theoretical upper-limit. Modeling error, noise, and nonlinearities would all act to reduce the achievable frame rate.

REFERENCES

[1] K. E. Lukong, K. Chang, E. W. Khandjian, and S. Richard, "RNA binding proteins in human genetic disease," *Trends in Genetics*, vol. 24, no. 8, pp. 416–425, May 2008.

[2] Z. Szolnoki, J. Serly, A. Kondacs, Y. Mandi, and F. Somogyvari, "Evaluation of the genetic variants of kinesin motor protein in ischemic stroke," *Journal of Stroke and Cerebrovascular Diseases*, vol. 18, no. 5, pp. 360–362, Sep 2009.

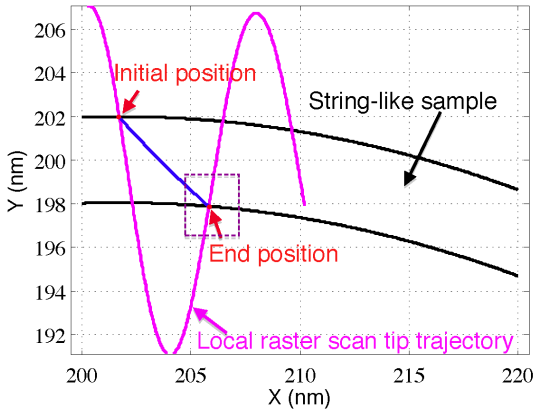

(a) Time optimal tip trajectory

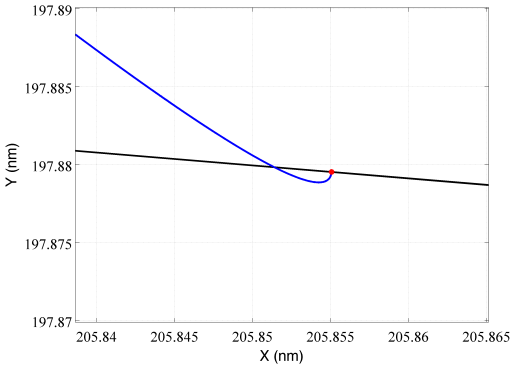

(b) Zoom in

Fig. 8. Illustration of the optimal time tip trajectory. (b) is the zoom in plot inside the purple dashed rectangular in (a).

[3] A. Yildiz, J. N. Forkey, S. A. McKinney, T. Ha, Y. E. Goldman, and P. R. Selvin, "Myosin V walks hand-over-hand: Single fluorescent imaging with 1.5-nm localization," *Science*, vol. 300, pp. 2061–2065, June 2003.

[4] C. Kural, H. Kim, S. Syed, G. Goshima, V. I. Gelfand, and P. R. Selvin, "Kinesin and dynein move a peroxisome in vivo: A tug-of-war or coordinated movement?" *Science*, vol. 308, no. 5727, p. 759C765, June 2005.

[5] Z. Wang, L. Millet, M. Mir, H. Ding, S. Unarunotai, J. Rogers, M. U. Gillette, and G. Popescu, "Spatial light interference microscopy (SLIM)," *Optics Express*, vol. 19, no. 2, pp. 1016–1026, Jan 2011.

[6] K. Svoboda, C. F. Schmidt, B. J. Schnapp, and S. M. Block, "Direct observation of kinesin stepping by optical trapping interferometry," *Nature*, vol. 365, pp. 721 – 727, Oct 1993.

[7] M. L. Walker, S. A. Burgess, J. R. Sellers, F. Wang, J. A. Hammer, J. Trinick, and P. J. Knight, "Two-headed binding of a processive myosin to F-actin," *Nature*, vol. 405, no. 6788, pp. 804–807, June 2000.

[8] N. Kodera, D. Yamamoto, R. Ishikawa, and T. Ando, "Video imaging of walking myosin V by high-speed atomic force microscopy," *Nature*, vol. 468, pp. 72–76, Oct 2010.

[9] O. H. Willemsen, M. M. E. Snel, A. Cambi, J. Greve, B. G. D. Grooth, and C. G. Figdor, "Biomolecular interactions measured by atomic force microscopy," *Review of Scientific Instruments*, vol. 79, no. 6, pp. 3267–3281, Dec 2000.

[10] M. B. Viani, L. I. Pietrasanta, J. B. Thompson, A. Chand, I. C. Gebeshuber, J. H. Kindt, M. Richter, H. G. Hansma, and P. K. Hansma, "Probing protein–protein interactions in real time," *Nature Structural Biology*, vol. 7, no. 8, pp. 644–647, Aug 2000.

[11] T. Ando, T. Uchihashi, N. Kodera, D. Yamamoto, A. Miyagi, M. Taniguchi, and H. Yamashita, "High-speed AFM and nano-visualization of biomolecular processes," *Eur J Physiol*, vol. 456, pp. 211–225, Dec 2008.

[12] G. Schitter and M. J. Rost, "Scanning probe microscopy at video-rate," *Materials Today, Microscopy special issue*, pp. 40–48, 2009.

[13] G. E. Fantner, G. Schitter, J. H. Kindt, T. Ivanov, K. Ivanova, R. Patel, N. Holten-Andersen, J. Adams, P. J. Thurner, I. W. Rangelow, and P. K. Hansma, "Components for high speed atomic force microscopy," *Ultramicroscopy*, vol. 1, no. 15, pp. 1–7, Jan 2004.

[14] G. Schitter, F. Allgower, and A. Stemmer, "A new control strategy for high-speed atomic force microscopy," *Nanotechnology*, vol. 15, pp. 108–114, Nov 2004.

[15] S. M. Salapaka, A. Sebastian, J. P. Cleveland, and M. V. Salapaka, "High bandwidth nano-positioner: A robust control approach," *Review of Scientific Instruments*, vol. 73, no. 9, pp. 3232–3241, September 2002.

[16] L. M. Picco1, L. Bozec, A. Ulcinas, D. J. Engledew, M. Antognozzi, M. A. Horton, and M. J. Miles, "Breaking the speed limit with atomic force microscopy," *Nanotechnology*, vol. 18, pp. 1–4, Dec 2006.

[17] S. Salapaka, T. De, and A. Sebastian, "Sample-profile estimate for fast atomic force microscopy," *Applied Physics Letters*, vol. 87, p. 053112 (3 pages), July 2005.

[18] P. Chang, P. Huang, J. Maeng, and S. Andersson, "Local raster scanning for high speed imaging of biopolymers in atomic force microscopy," *Review of Scientific Instruments*, vol. 82, no. 6, p. 063703 (7 pages), June 2011.

[19] P. Huang and S. B. Andersson, "Generating images from non-raster data," in *Proceedings of the American Control Conference*, San francisco, CA, June 2011, pp. 2246–2251.

[20] D. Y. Abramovitch, S. B. Andersson, L. Y. Pao, and G. Schitter, "A tutorial on the mechanisms, dynamics, and control of atomic force microscopes," in *Proceedings of the 2007 American Control Conference*. New York City, USA: American Control Conference, July 2007, pp. 3488–3502.

[21] H. Adriaens, D. Koning, and R. Banning, "Modeling piezoelectric actuators," *Mechatronics, IEEE/ASME Transactions on*, vol. 5, no. 4, pp. 331 – 341, Dec 2000.

[22] P. R. Dahl and R. Wilder, "Math model of hysteresis in piezo-electric actuators for precision pointing system," in *Proceedings of the Eighth Annual Rocky Mountain Conference*. Keystone, CO, UNITED STATES: Guidance and control 1985, Feb 1985, pp. 61–88.

[23] B. Mokaberi and A. Requicha, "Compensation of scanner creep and hysteresis for afm nanomanipulation," *Automation Science and Engineering, IEEE Transactions on*, vol. 5, no. 2, pp. 197 – 206, Apr 2008.

[24] F. L. Lewis and V. L. Syrmos, *Optimal control*. John Wiley and Sons, INC., 1995.

[25] Z. Shen and S. B. Andersson, "Minimum time control of a second order system." IEEE Conference on Decision and Control, Dec 2010, pp. 4819–4824.

[26] M. L. Workman, R. L. Kosut, and G. F. Franklin, "Adaptive proximate time-optimal servomechanisms: Continuous time case." American Control Conference, June 1987, pp. 589–594.

[27] B. J. Kenton, A. J. Fleming, and K. K. Leang, "Compact ultra-fast vertical nanopositioner for improving scanning probe microscope scan speed," *Review of Scientific Instruments*, vol. 82, p. 123703 (8 pages), June 2011.